Phase-Space Dynamics of Ionization Injection in Plasma-Based Accelerators

X. L. Xu,[1] J. F. Hua,[1] F. Li,[1] C. J. Zhang,[1] L. X. Yan,[1] Y. C. Du,[1] W. H. Huang,[1] H. B. Chen,[1] C. X. Tang,[1] W. Lu,[1,2,*] P. Yu,[2] W. An,[2] C. Joshi,[2] and W. B. Mori[2]
[1]Department of Engineering Physics, Tsinghua University, Beijing 100084, China
[2]University of California Los Angeles, Los Angeles, California 90095, USA
(Received 27 April 2013; published 23 January 2014)

The evolution of beam phase space in ionization injection into plasma wakefields is studied using theory and particle-in-cell simulations. The injection process involves both longitudinal and transverse phase mixing, leading initially to a rapid emittance growth followed by oscillation, decay, and a slow growth to saturation. An analytic theory for this evolution is presented and verified through particle-in-cell simulations. This theory includes the effects of injection distance (time), acceleration distance, wakefield structure, and nonlinear space charge forces, and it also shows how ultralow emittance beams can be produced using ionization injection methods.

DOI: 10.1103/PhysRevLett.112.035003 PACS numbers: 52.38.Kd, 41.75.Jv, 52.35.Mw

Research on wakefield accelerators driven by the propagation of ultrashort high power lasers or intense relativistic charged particle beam pulses through plasma has made great strides in the past decade [1]. In the laser driver case, energy gains up to 2 GeV and energy spreads of a few percent have been achieved using centimeter scale plasmas [2–6]; in the beam driver case, an energy gain more than 42 GeV has been demonstrated in a meter-scale plasma [7–9]. These have inspired great interest in plasma wave wakefield accelerators worldwide as drivers for compact coherent light sources for science and technology, on the one hand, and TeV-class colliders with much smaller footprint than the current rf-based accelerators for high energy physics, on the other hand. However, these applications require beams that have extremely small transverse and longitudinal emittances or phase-space area, which is formally defined as $\epsilon_N = \sqrt{\langle x^2\rangle\langle p_x^2\rangle - \langle x p_x\rangle^2}/mc$, where $\langle\cdot\rangle$ represents an ensemble average over the electron phase-space distribution. Therefore, the next challenge for plasma accelerators is to perfect methods for controlled injection of charge in the wake that can produce such low emittance beams.

Many novel methods for controlled injection have been proposed and demonstrated, such as injection by using plasma density ramps [10], by colliding laser pulses [11], and by ionization-induced injection [5,12–17]. In ionization injection, electrons are produced inside the wake by tunneling ionization by the electric field of laser pulse or by the combined field of the beam driver and the wake, where they can be more easily captured and accelerated. Recent computational work [18–20] including both self-consistent simulations and tracking of particles in prescribed fields has shown that 10 nm emittances may be achievable through ionization injection. However, the ultimate emittance is determined from a complex six-dimensional phase dynamics which needs to be better understood. This area of research is, therefore, of fundamental importance for achieving beam quality well beyond what is achievable with current technology.

In this Letter, we examine the effects that affect the beam phase-space evolution of electrons in ionization-induced injection within plasma wakes using a combination of theory and simulations. We find that there are three distinct stages in this evolution and that each stage can impact the final beam quality. In a typical case where the injection time is limited to few inverse plasma periods ($2\pi\omega_p^{-1}$) and the charge is low, these three stages are as follows. First, when ionization is occurring, the emittance of the injected beam grows quickly in time from the initial thermal emittance. Second, immediately following ionization, the emittance slowly decreases to a minimum value. Finally, the emittance again gradually increases to a saturated value. If the ionization time is more than $\sim\pi\omega_p^{-1}$, the emittance grows to the saturated level during the first stage including an oscillatory behavior before it slowly decreases. In the "high" charge limit the emittance evolves monotonically towards the same saturated value.

The theory reveals that the evolution in emittance described above is due to a complex longitudinal and transverse phase mixing process of electrons born at different times. The derived expressions clearly show how the emittance depends on different physical parameters, e.g., injection distance, acceleration distance, wakefield structure, and nonlinear self-forces. The predictions are compared against results from OSIRIS [21] particle-in-cell (PIC) simulations and good agreement is obtained.

To understand the emittance evolution, we first analyze the single particle motion using the equation of motion for a charged particle undergoing acceleration and betatron motion [22] in a nonlinear wake excited in the blowout regime [23–25],

$$\ddot{\vec{x}}_\perp + \frac{\dot{\gamma}}{\gamma}\dot{\vec{x}}_\perp + k_\beta^2 \vec{x}_\perp = 0, \tag{1}$$

where $\vec{x}_\perp$ are the transverse coordinates of the particle, the overdot refers to derivative with respect to $s \equiv z$, the propagation distance, and $k_\beta = k_p/\sqrt{2\gamma}$ is the betatron wave number. We use s together with the new variable $\xi \equiv ct - z$ which defines the longitudinal position of the particle inside the wake. For a relativistic particle ξ remains nearly constant and $s = ct$. In the limit $\ddot{\gamma} \ll k_\beta \dot{\gamma}$ and $\dot{\gamma} \ll k_\beta \gamma$, Eq. (1) has a general asymptotic solution of the form $\vec{x}_\perp = (\vec{x}_{\perp 0}/\gamma^{1/4}) e^{i\int dsk_\beta}$. In addition, exact solutions for Eq. (1) can be found for specific cases such as when $\dot{\gamma} = \text{const} = qE_z/mc^2$, which is reasonable when phase slippage is not important. For this case, Eq. (1) becomes

$$\ddot{x} + \frac{E_z}{\gamma_0 + E_z s}\dot{x} + \frac{x}{2(\gamma_0 + E_z s)} = 0, \tag{2}$$

where $\gamma(s) = \gamma_0 + E_z s$, and we normalize position to k_p^{-1}, time to ω_p^{-1}, E_z to $mc\omega_p/e$, and charge to e. Exact and asymptotic solutions for Eq. (2) are

$$x = c_1 J_0\left(\sqrt{\frac{2\gamma}{E_z^2}}\right) + c_2 Y_0\left(\sqrt{\frac{2\gamma}{E_z^2}}\right) \approx C\left(\frac{2E_z^2}{\pi^2\gamma}\right)^{1/4} \cos\Phi, \tag{3}$$

$$\dot{x} = -\sqrt{\frac{1}{2\gamma}}\left[c_1 J_1\left(\sqrt{\frac{2\gamma}{E_z^2}}\right) + c_2 Y_1\left(\sqrt{\frac{2\gamma}{E_z^2}}\right)\right] \approx -C\left(\frac{E_z^2}{2\pi^2\gamma^3}\right)^{1/4} \sin\Phi, \tag{4}$$

where $\Phi = (\sqrt{2\gamma} - \sqrt{2\gamma_0})/E_z$ is the betatron phase. The asymptotic solutions are of the general form with $\Phi = \int ds/\sqrt{2\gamma}$. Direct comparison with single particle and PIC simulations shows that the asymptotic expressions are valid with high accuracy when $\gamma \gtrsim 2$ [26].

We consider the x-p_x phase space corresponding to one of the two transverse directions. Electrons are defined by their ionization time s_i and initial phase-space location $(x_0(s_i), p_{x0}(s_i))$. In addition, electrons of interest are rapidly accelerated as they reach a longitudinal position ξ_f in the wake where they remain phase locked and thus feel a constant E_z. As we show later, electrons ionized at the same s_i can reside over the full range of ξ_f within the bunch (we call this longitudinal phase mixing), and thus feel a range of E_z which we define as δE_z. We also assume that each electron begins at rest and the rapid interaction with the incoming laser leads to a small natural spread in p_x. This "thermal" spread can thus be neglected.

We integrate Eq. (2) for many test electrons. To model the effect of δE_z, the E_z of each electron is randomly chosen from 0.9 to 1.1. In Fig. 1(a) we show electrons ionized at different times. After a group of electrons is ionized they begin to rotate in x-p_x phase space. The first group (red) has a betatron phase Φ_M, and the most recent group (purple) has a phase Φ_m. If ionization continues, then $\Phi_m = 0$. Clearly, the area in phase space increases during the injection process due to each group of electrons having a different betatron phase; we call this transverse phase mixing.

In Fig. 1(b) we show the phase space at a " time" after the ionization has stopped. For simplicity, we consider a case where the injection time $\Delta s < \pi$. However, electrons at Φ_M have a higher energy (due to being accelerated for a longer time) and hence lower betatron frequency than those electrons at Φ_m. As a result, $\Phi_M - \Phi_m \equiv \Delta\Phi$ gradually decreases and hence the emittance gradually decreases.

Later in time, due to any spread in E_z, the electrons ionized at the same time develop a spread in phase. Eventually, the electrons at Φ_M (Φ_m) are those injected first (last) but which have experienced the smallest (largest) E_z. In this case, electrons at Φ_M now rotate faster than those at Φ_m, causing the emittance to gradually increase.

It turns out that a simple expression for the above emittance evolution process can be obtained if one assumes that the phase-space distribution is independent of Φ in a sector as shown, for example, by the dotted lines in Fig. 1(c). From Eqs. (3) and (4), one can see that the phase-space coordinates (x, p_x) depend very weakly on particle energy $(\sim\gamma^{1/4})$; therefore, for a given time, we can assume $x = x_0(\gamma_0/\bar{\gamma})^{1/4}\cos\Phi$, $p_x = x_0(\gamma_0\bar{\gamma})^{1/4}\sin\Phi/\sqrt{2}$, where the $\bar{\gamma}$ is the average energy of the injected particles at this time. We can obtain $\langle x^2\rangle = \sigma_{x0}^2(\gamma_0/\bar{\gamma})^{1/2}[1 + (\sin 2\Phi_M - \sin 2\Phi_m)/(2\Phi_M - 2\Phi_m)]/2$, $\langle p_x^2\rangle = \sigma_{x0}^2(\gamma_0\bar{\gamma})^{1/2}[1 - (\sin 2\Phi_M - \sin 2\Phi_m)/(2\Phi_M - 2\Phi_m)]/4$, and $\langle x p_x\rangle = (\sigma_{x0}^2\gamma_0^{1/2})(\cos 2\Phi_M - \cos 2\Phi_m)/(\Phi_M - \Phi_m)/4\sqrt{2}$, where

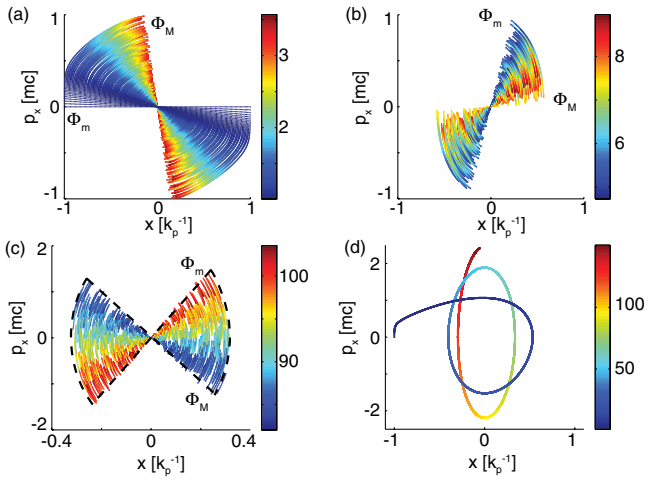

FIG. 1 (color online). Phase-space snapshots from single particle model illustrating the transverse phase mixing process. (a)–(c) x-p_x phase space at different times: (a) $t = 3\,(\omega_p^{-1})$ when the ionization is just terminated, (b) $t = 8$, (c) $t = 94$. (d) x-p_x phase-space trajectory for a typical particle, where the color represents the relativistic factor γ. Note that at early time, γ is correlated with the ionization time s_i.

$\sigma_{x0}^2 = \int x_0^2 f(x_0) dx_0$ and $f(x_0)$ is the normalized distribution function when the electrons are born. Therefore, the normalized emittance

$$\epsilon_N(\Delta\Phi) = \sqrt{\langle x^2\rangle\langle p_x^2\rangle - \langle x p_x\rangle^2} = \epsilon_{sat}\sqrt{1 - \left(\frac{\sin\Delta\Phi}{\Delta\Phi}\right)^2}, \quad (5)$$

where $\Delta\Phi \approx \sqrt{2(E_{zm}z_M + 1)}/E_{zm} - \sqrt{2(E_{zM}z_m + 1)}/E_{zM}$, $z_{M,m} = s - s_{iM,m}$, and $s_{iM,m}$ refers to when electrons at M, m were ionized, $\epsilon_{sat} = \sigma_{x0}^2/2\sqrt{2}$ is the value of the emittance when the phase ellipse is filled out, in real units,

$$\epsilon_{sat}[\mu\mathrm{m}] = \frac{1}{2\sqrt{2}} k_p[\mu\mathrm{m}^{-1}]\sigma_{x0}^2[\mu\mathrm{m}^2]. \quad (6)$$

If we neglect δE_z, which is reasonable early in time, and assume injection is still occurring ($z_m = 0$) and $\Delta\Phi < 1$, then

$$\epsilon_N \approx \epsilon_{sat}\frac{\Delta\Phi}{\sqrt{3}} \approx \epsilon_{sat}\sqrt{\frac{2}{3}}\frac{\sqrt{1 + E_z z} - 1}{E_z}, \quad (7)$$

which shows that ϵ_N grows with propagation distance.

After the injection terminates, the injected electrons continue their betatron oscillations. For each injected electron $\Phi \gg 1$ and $\delta\Phi \equiv \Phi - \langle\Phi\rangle \ll \Phi$, $\Phi = (\sqrt{2\gamma} - \sqrt{2\gamma_0})/E_z$ and $\gamma = \gamma_0 + E_z z$, leading to $\delta\Phi/\Phi \approx (\delta z/z - \delta E_z/E_z)/2$. The variance of $\delta\Phi$ can be obtained by assuming the independence between the accelerating field and the injection time,

$$\sigma_\Phi \equiv \sqrt{\langle\delta\Phi^2\rangle} \approx \sqrt{\frac{1}{2E_z}\left[\frac{\sigma_z^2}{z} + z\left(\frac{\sigma_{E_z}}{E_z}\right)^2\right]}, \quad (8)$$

where $\sigma_z^2 = \langle(s_i - \langle s_i\rangle)^2\rangle$ and $\sigma_{E_z}^2 = \langle(E_z - \langle E_z\rangle)^2\rangle$. To obtain an expression of $\Delta\Phi$ in terms of σ_Φ, a certain distribution of electrons needs to be assumed. For a uniform distribution, $\Delta\Phi = \sqrt{12}\sigma_\Phi$, Eq. (5) then becomes

$$\epsilon_N = \epsilon_{sat}\sqrt{1 - \left(\frac{\sin\sqrt{12}\sigma_\Phi}{\sqrt{12}\sigma_\Phi}\right)^2}. \quad (9)$$

Equations (8) and (9) predict that for $z < (E_z/\sigma_{E_z})\sigma_z \equiv z_0$ the emittance actually decreases; it reaches a local minimum at z_0, and then increases until it saturates at ϵ_{sat}. Therefore, to achieve the minimal emittance, the acceleration distance should be optimized to be close to z_0.

We next compare these predictions against self-consistent 2D OSIRIS simulations of injection triggered by a laser pulse into the wake produced by an electron beam [18–20]. In the sample simulations the laser is copropagating with the wake. As schematically shown in Fig. 2(a), in the simulation the beam driver propagates in a mixture of a plasma with a density $n_p = 1.6 \times 10^{17}\,\mathrm{cm}^{-3}$ and neutral He gas of density $n_{\mathrm{He}} = 1.6 \times 10^{13}\,\mathrm{cm}^{-3}$. The simulation used a 5000×4000 cell grid and 2 and 4 particles per cell for the plasma and neutral He, respectively. In Fig. 2(b) the evolution of the emittance in the simulation and the predictions of Eq. (5) (during ionization) and Eq. (9) (after ionization) using σ_z and σ_{E_z} calculated from the simulation are compared, and the agreement is very good. The simulation curve also oscillates in time immediately after the rapid increase. In this case the ionization duration is limited by the Rayleigh length of the laser and is $\sim 0.6\,\mathrm{ps} > \pi\omega_p^{-1}$. Therefore, the first group of electrons that are ionized will have rotated through more than an angle of π in x-p_x phase space. This is illustrated in Fig. 1(d) where the trajectory in x-p_x space of an electron born at rest is shown. As it is accelerated its betatron frequency and amplitude in x decreases while its amplitude in p_x increases. As a result, the edge of the phase space for a collection of electrons is made up of layers of groups of electrons corresponding to each $\pi\omega_p^{-1}$ of injection. Each group corresponds to an ellipse with a different aspect ratio, and each ellipse has edge in phase space given by the trajectory shown in Fig. 1(d), as can be seen in Fig. 2(c). The area in phase space will therefore oscillate at twice the betatron frequency. After several oscillations, the particles become smeared out in x-p_x phase space and the oscillations damp away. In Fig. 2(d) we show x-p_x for $z = z_0$ where the emittance reaches its minimum, and it can be clearly seen that the range of $\Delta\Phi < \pi/2$ at this time, even though $\Delta\Phi \approx 3\pi/2$ at the end of injection.

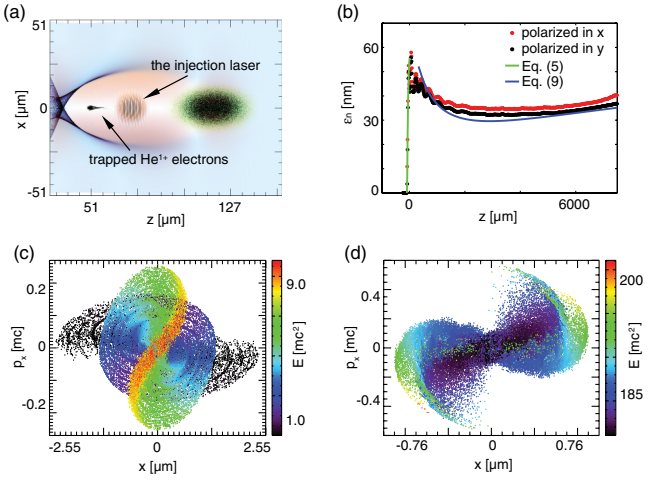

FIG. 2 (color online). (a) 2D PIC simulation of ionization injection by a laser into a beam driven wake. Drive beam (green): $\sigma_r = 15\,\mu\mathrm{m}, \sigma_z = 25\,\mu\mathrm{m}, n_b = 2.6 \times 10^{17}\,\mathrm{cm}^{-3}, E_b = 2\,\mathrm{GeV}$. Laser: $\lambda = 800$ nm, $a_0 = 0.04$, $w_0 = 3\,\mu$m, $\tau \approx 30$ fs. (b) Comparison of the emittance evolution between simulations and theory. The red line and the black line are for the laser polarized in or out of the simulation plane, respectively. The x-p_x phase space when the injection is terminated (c) and when $z = z_0$ (d).

Equations (8) and (9) are based on Eq. (2), where space charge forces are neglected. For relatively large injected charge, the nonlinear space charge force in both the longitudinal and transverse directions of the injected electrons could modify the trajectories of the electrons while they are at low energy, thereby modifying the evolution of the emittance. For cases where the total injection phase is larger than π, space charge effects lead directly to a saturation of the emittance around ϵ_{sat}. In Fig. 3(a) this saturation behavior can be clearly seen. The quadratic dependence of ϵ_{sat} on the laser spot size is also verified through PIC simulations with a good agreement [Fig. 3(b)]. For cases where the total injection phase is much less than π, Eq. (5) suggests that very small emittance can be achieved. In Fig. 3(a) the emittance evolution of a simulation in which the ionization time was much shortened by reducing the length of the region of neutral He is shown (green curve). To control the total injected charge, the neutral He density is increased proportionally in the simulations. One can see that the initial emittance is much reduced, and the emittance slowly increases during the acceleration process (at low charge it does not increase). However, the increase of total projected emittance is mainly due to the difference of accelerating field within the bunch, and on each slice the emittance remains invariant even with the effect of the space charge force. The dominant space charge effect is the longitudinal expansion of the beam leading to a larger spread in the accelerating field. Therefore, if the beam load can be optimized to flatten the wake, the projected emittance can be better controlled [27,28].

The slice emittance can also be affected by a longitudinal mixing process occurring in the injection stage. Electrons ionized at different times (and different transverse locations) can reside within the same longitudinal beam slice through this mixing. Furthermore, this can lead to different phase-space distributions including a spread in initial energy, thereby leading to transverse mixing within a slice. This is a fundamentally different situation compared to the phase mixing process in traditional accelerators [29]. This mixing can be described by a trapping condition in [14]. This injection condition can be approximated as $\delta\psi \approx -1$, where $\psi \equiv (e/mc^2)(\varphi - v_\varphi/cA_z)$, and ψ in the ion channel can be expressed as $\psi(\xi, r) \approx [r_b^2(\xi) - r^2]/4$, where $r_b(\xi)$ is the normalized radius of the ion channel and it has a spherical shape for sufficiently large blowout radius r_m, i.e., $r_b^2(\xi) = r_m^2 - \xi^2$ [23–25]. The final relative longitudinal position of each injected electron can be obtained by applying $\delta\psi \approx -1$:

$$\xi_f \approx \sqrt{4 + \xi_i^2 + r_i^2 - r_f^2}, \tag{10}$$

where $r_m > 2$ is implicitly required. In many cases, r_i and r_f can be neglected since $r_i, r_f \ll 1$. An electron's initial position is defined by (ξ_i, r_i, s_i), and the distribution of electrons in ξ_i will vary with r_i and s_i depending on the laser transverse and longitudinal profiles (including its focusing optics). Therefore, each final slice of the injected beam is composed of the electrons ionized at different longitudinal positions, different transverse locations, and different times. This also leads to the electrons within a slice having different energies (when they are trapped and initially accelerated) and each slice having a different phase-space distribution. In Fig. 4(a) we plot the relation between ξ_f and ξ_i at a propagation distance of $z \approx 1$ mm from a PIC simulation with a Gaussian-shaped laser and compare with our theoretical estimate (where r_i and r_f were neglected), and a similar trend is seen. In Fig. 4(b) we plot the relation between ξ_f and initial $r = x$ of each electron, with each color representing a different birth time. One can see clearly that the equal-time contours have a U shape, and this is mainly due to the Gaussian intensity profile. From the color code of both Figs. 4(a)and 4(b), electrons born at the same time are seen to be distributed into each slice. In the theory curves of Fig. 2(b) we used the initial phase-space distributions from the self-consistent simulations which included longitudinal mixing.

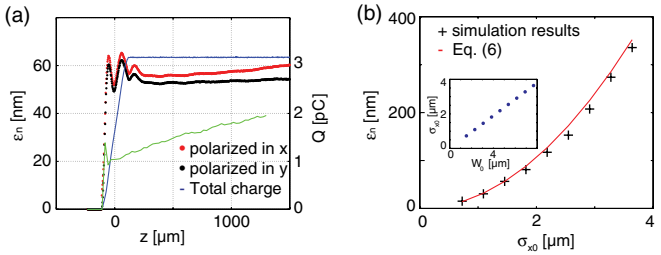

FIG. 3 (color online). (a) Emittance evolution with space charge effect. The red line and the black line show the emittance evolution for the laser in or out of the 2D simulation plane, respectively, with $n_{\mathrm{He}} = 1.6 \times 10^{16}\,\mathrm{cm}^{-3}$. The green line shows the emittance evolution for limited helium range (19 μm), $n_{\mathrm{He}} = 1.6 \times 10^{17}\,\mathrm{cm}^{-3}$. The charge value (blue curve) is estimated by assuming the beam is symmetric in 3D. (b) The quadratic dependence of the saturated emittances on σ_{x0} for large injection phase ($> \pi$) with space charge effect. The laser intensity was fixed at $a_0 = 0.04$ for different spot sizes, and the inner plot shows the dependence of σ_{x0} on the laser spot size.

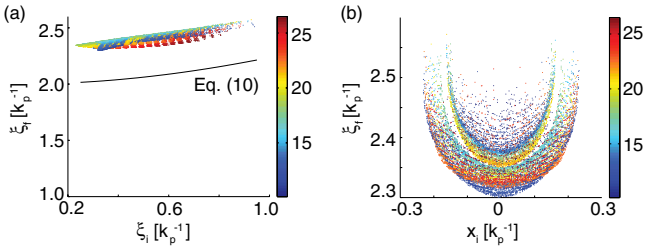

FIG. 4 (color online). (a) The dependence of ξ_f on ξ_i from simulation and the comparison with theoretical estimation. (b) The dependence of ξ_f on x_i. Note that different colors represent different electron birth times.

In summary, the evolution of beam phase space in ionization injection in plasma wakefields is analyzed using theory and simulations. Two key phase mixing processes, namely, longitudinal and transverse phase mixing, are found to be responsible for the complex emittance dynamics that shows initial rapid growth followed by oscillation, decay, and a slow growth to saturation. An analytic theory is developed to include the effects of injection distance (time), acceleration distance, wakefield structure, and nonlinear space charge forces. Formulas for the emittance in the low and high charge regimes are presented and verified through PIC simulations with good agreement.

Work supported by NSFC Grant No. 11175102, the National Basic Research Program of China Grant No. 2013CBA01501, Tsinghua University Initiative Scientific Research Program, the Thousand Young Talents Program, NSFC Grant No. 11005063, DOE Grants No. DE-FG02-92-ER40727, No. DE-SC0008491, and No. DE-SC0008316, and NSF Grants No. PHY-0936266 and No. PHY-0960344. Simulations are performed on Hoffman and Dawson2 clusters at UCLA and NERSC at LBNL.

*weilu@tsinghua.edu.cn

[1] E. Esarey, C. B. Schroeder, and W. P. Leemans, Rev. Mod. Phys. **81**, 1229 (2009).
[2] W. P. Leemans, B. Nagler, A. J. Gonsalves, Cs. Tóth, K. Nakamura, C. G. R. Geddes, E. Esarey, C. B. Schroeder, and S. M. Hooker, Nat. Phys. **2**, 696 (2006).
[3] S. Kneip *et al.*, Phys. Rev. Lett. **103**, 035002 (2009).
[4] D. H. Froula *et al.*, Phys. Rev. Lett. **103**, 215006 (2009).
[5] C. E. Clayton *et al.*, Phys. Rev. Lett. **105**, 105003 (2010).
[6] X. Wang *et al.*, Nat. Commun. **4**, 1988 (2013).
[7] P. Muggli *et al.*, Phys. Rev. Lett. **93**, 014802 (2004).
[8] M. J. Hogan *et al.*, Phys. Rev. Lett. **95**, 054802 (2005).
[9] I. Blumenfeld *et al.*, Nature (London) **445**, 741 (2007).
[10] C. Geddes, K. Nakamura, G. Plateau, Cs. Toth, E. Cormier-Michel, E. Esarey, C. Schroeder, J. Cary, and W. Leemans, Phys. Rev. Lett. **100**, 215004 (2008).
[11] X. Davoine, E. Lefebvre, C. Rechatin, J. Faure, and V. Malka, Phys. Rev. Lett. **102**, 065001 (2009).
[12] E. Oz *et al.*, Phys. Rev. Lett. **98**, 084801 (2007).
[13] T. P. Rowlands-Rees *et al.*, Phys. Rev. Lett. **100**, 105005 (2008).
[14] A. Pak, K. A. Marsh, S. F. Martins, W. Lu, W. B. Mori, and C. Joshi, Phys. Rev. Lett. **104**, 025003 (2010).
[15] C. McGuffey *et al.*, Phys. Rev. Lett. **104**, 025004 (2010).
[16] J. S. Liu *et al.*, Phys. Rev. Lett. **107**, 035001 (2011).
[17] B. B. Pollock *et al.*, Phys. Rev. Lett. **107**, 045001 (2011).
[18] B. Hidding, G. Pretzler, J. B. Rosenzweig, T. Königstein, D. Schiller, and D. L. Bruhwiler, Phys. Rev. Lett. **108**, 035001 (2012).
[19] F. Li *et al.*, Phys. Rev. Lett. **111**, 015003 (2013).
[20] Y. Xi, B. Hidding, D. Bruhwiler, G. Pretzler, and J. B. Rosenzweig, Phys. Rev. ST Accel. Beams **16**, 031303 (2013).
[21] P. M. A. Sloot, A. G. Hoekstra, C. J. K. Tan, and J. J. Dongarra, Lect. Notes Comput. Sci. **2331**, 342 (2002).
[22] S. Wang *et al.*, Phys. Rev. Lett. **88**, 135004 (2002).
[23] W. Lu, C. Huang, M. Zhou, W. B. Mori, and T. Katsouleas, Phys. Rev. Lett. **96**, 165002 (2006).
[24] W. Lu, C. Huang, M. Zhou, M. Tzoufras, F. S. Tsung, W. B. Mori, and T. Katsouleas, Phys. Plasmas **13**, 056709 (2006).
[25] W. Lu, M. Tzoufras, C. Joshi, F. Tsung, W. Mori, J. Vieira, R. Fonseca, and L. Silva, Phys. Rev. ST Accel. Beams **10**, 061301 (2007).
[26] A more detailed discussion will be presented in a future publication.
[27] M. Tzoufras, W. Lu, F. Tsung, C. Huang, W. Mori, T. Katsouleas, J. Vieira, R. Fonseca, and L. Silva, Phys. Rev. Lett. **101**, 145002 (2008).
[28] M. Tzoufras, W. Lu, F. S. Tsung, C. Huang, W. B. Mori, T. Katsouleas, J. Vieira, R. A. Fonseca, and L. O. Silva, Phys. Plasmas **16**, 056705 (2009).
[29] L. Serafini and J. B. Rosenzweig, Phys. Rev. E **55**, 7565 (1997).